


 CrossMark
click for updates

 Cite this: *New J. Chem.*, 2014,
38, 4774

Precursor-driven selective synthesis of hexagonal chalcocite (Cu₂S) nanocrystals: structural, optical, electrical and photocatalytic properties†

 Gopinath Mondal,^a Pradip Bera,^a Ananyakumari Santra,^a Sumanta Jana,^b
Tarak Nath Mandal,^c Anup Mondal,^b Sang Il Seok^{cd} and Pulakesh Bera^{*a}

The reaction of CuCl₂·2H₂O with the methyl ester of 3,5-dimethyl pyrazole-1-dithioic acid (mdpa) yields a blackish brown complex of composition, [Cu(mdpa)₂][CuCl₂]. The complex formed a well-defined crystal and is characterized by single-crystal X-ray diffraction, thermogravimetry (TG), and spectroscopic studies. The molecule possesses a distorted tetrahedral configuration with a CuN₂S₂ chromophore with +1 oxidation state of copper. The TG study reveals that the molecule is a suitable precursor for copper sulfide nanoparticles. The low temperature thermal decomposition of the single-source precursor produces hexagonal chalcocite (Cu₂S) nanostructures in ethylene diamine and ethylene glycol. A selective synthesis of copper-rich high chalcocite was obtained using the new precursor. The size and morphology of the synthesized Cu₂S nanoparticles are guided by the precursor and likely to be less dependent on the solvent used in the experiment. The nanoparticles were characterized by X-ray diffraction, scanning electronic microscope, and UV-Vis spectroscopic studies. The optical band gap of the as-synthesized Cu₂S nanoparticles is measured to be 1.80–2.40 eV. The Cu₂S nanoparticles are found to be good catalysts in UV photo catalytic decomposition (90%) of Congo red (CR) dye following first-order reaction kinetics, and the reusability study of the Cu₂S catalyst also shows excellent catalytic performance (80%).

 Received (in Montpellier, France)
15th April 2014,
Accepted 7th July 2014

DOI: 10.1039/c4nj00584h

www.rsc.org/njc

1. Introduction

Recently, the development of a single-source molecular precursor for the preparation of binary and ternary semiconductor nanocrystals (NCs) has been attracting considerable attention as a single-source precursor (SP) route, providing special key advantages over the other conventional methods for preparing inorganic powders, nanoparticles, and thin films. First, the single-source precursors can be easily obtained in ambient conditions. These are mostly metal-organic or organometallic compounds, which have century-long advanced science. Second, the protocol of a single-source route is based on the advantages

of mildness, safety and a simplified one-pot synthesis of NCs.^{1–3} Lastly, the presence of all constituent elements in required atomic ratios is chemically maintained in a SP strategy, which offers a clean synthetic method to produce pure compounds. The ease of synthesis of single-source precursors in ambient conditions popularizes the use of it in the preparation of semiconductor chalcogenides.

Copper sulfide (Cu_xS, where $x = 1$ to 2) is one of the chalcogenides that has received considerable attention in recent years, owing to wide stoichiometric compositions, nanocrystal morphologies and hierarchical structure. The stoichiometric composition of copper sulfide varies from copper-rich Cu₂S to copper deficient CuS₂ such as Cu₂S, Cu_{1.96}S, Cu_{1.94}S, Cu_{1.8}S, Cu_{1.75}S, and CuS with varying morphologies⁴ and different unique optoelectronics properties.^{5–7} The band gap of copper sulfide can vary in a wider range (1.2–2.5 eV) with stoichiometric composition, which makes it a highly desirable material for solar cells,^{8,9} nonvolatile memory devices,¹⁰ nano-scale switches,¹¹ lithium ion batteries,¹² gas sensing^{13,14} and theranostic applications.¹⁴

In the literature, several SP strategies have been used for the synthesis of copper sulfide nanoparticles with different shapes and sizes and morphologies. For instance, Liu *et al.*¹⁵ decomposed Cu(S₂CNET₂)₂ in a mixture of dodecanethiol and oleic acid to obtained wires of hexagonal Cu₂S (chalcocite), while Lou

^a Post Graduate Department of Chemistry, Panskura Banamali College, Vidyasagar University, Midnapore (E), West Bengal-721152, India.

E-mail: pbera.pbc.chem@gmail.com

^b Department of Chemistry, Indian Institute of Engineering Science and Technology (IIST), Shibpur, West Bengal-711103, India

^c KRICT-EPFL Global Research Laboratory, Division of Advanced Materials, Korea Research Institute of Chemical Technology, 141 Gajeong-Ro, Yuseong-Gu, Daejeon 305-600, South Korea

^d Department of Energy Science, Sungkyunkwan University, Suwon 440-746, South Korea

† CCDC 996834. For crystallographic data in CIF or other electronic format see DOI: 10.1039/c4nj00584h

*et al.*¹⁶ decomposed $\text{Cu}(\text{S}_2\text{CNET}_2)_2$ in TOP/TOPO to obtain spherical $\text{Cu}_{1.8}\text{S}$ (digenite) nanocrystals. Corncoblike Cu_2S nanostructures were obtained through the thermolysis of copper dithiolate in dodecanethiol.¹⁷ Korgel *et al.* prepared Cu_2S nanorods, nanodiscs, and nanoplatelets by solvent-less thermolysis of a copper-alkylthiolato precursor.¹⁸ In another report, Li *et al.* synthesized monodispersed Cu_2S nanocrystals by the reaction of $\text{Cu}(\text{II})$ -stearate and dodecanethiol in 1-octadecene.¹⁹ The hydrothermal growth of CuS nanowires from Cu -dithioxamide was reported by Roy and Srivastava.²⁰ Almost all of the reported SP methods have been performed using hazardous external surfactants. Several factors, such as nature and concentration both of the precursor and capping agent have an influence on the rate of nucleation and growth, and hence the morphology of particles.^{21–24} Very recently, the Liberto Manna group reported the use of $\text{Cu}(\text{I})$ complex, $[\text{Cu}(\text{CH}_3\text{CN})_4]\text{PF}_6$, to prepare platelet-shape copper sulfide nanocrystals from covellite ($\text{Cu}_{1.1}\text{S}$) where $\text{Cu}:\text{S}$ ratio could be gradually increased from 1.1:1 to 2:1, retaining their overall size and morphology.²⁵ The same $\text{Cu}(\text{I})$ complex was also used by the same group to increase in Cu content of Cu_{2-x}Se NCs.²⁶ In each case, the $\text{Cu}(\text{I})$ complex, $[\text{Cu}(\text{CH}_3\text{CN})_4]\text{PF}_6$, helps to form copper-rich copper sulfide NCs, but the mechanism is unclear. In another report, Nair and Scholes concluded that SP derived from thiosemicarbazide, a NS chelate, are generally effective in evaluating anisotropic structure of the NCs where the ligand internally acts as the structure directing agent.²⁷ The use of functional molecules as capping ligands in SP to control the shape, size, and also the assembly structure of nanocrystallites in the solution-phase synthesis has been extensively studied. Therefore, the rational design and synthesis of ligands is very crucial for the preparation of SP that could be used to prepare the hierarchical structure of particles through the SP route. Moreover, the oxidation state of metal in SP has also a great influence on the final product. In the literature, the SP route to synthesize copper-rich Cu_2S or copper-deficient CuS in the presence of reducing agent(s) with varying morphologies and stoichiometries were obtained using mainly the metal-organic compounds of $\text{Cu}(\text{II})$.^{1–3,21–24} The reduction of $\text{Cu}(\text{II})$ to $\text{Cu}(\text{I})$ is required to form copper rich morphologies *e.g.*, $\text{Cu}_{1.8}\text{S}$, $\text{Cu}_{1.96}\text{S}$, Cu_2S *etc.*, and in most of the cases, the reducing agents/solvents were used to reduce the $\text{Cu}(\text{II})$ species to $\text{Cu}(\text{I})$. The effort to synthesize the functionalized SP where the oxidation state of copper is chemically maintained to +1 is practically rare. Consequently, the use of the $\text{Cu}(\text{I})$ complex is also limited to prepare copper-rich copper sulfide NCs. We report the synthesis of a new SP of heterocyclic NS-chelate where the oxidation state of copper in the SP is chemically maintained to +1. Further the SP is used in selective preparation of copper rich Cu_2S NCs without using any reducing agent.

In search of NS-chelates having ability to direct of particles morphology for NCs, we synthesize a new pyrazolyl ligand *mdpa* and its copper(I) complex, $[\text{Cu}(\text{mdpa})_2][\text{CuCl}_2]$. Pyrazolyl compounds are being considered as ancillary ligands due to their fascinating mode of coordination, which is reflected in the literature and text books of chemistry. Pyrazole (1, 2 diazole)

is isomeric with imidazole (1, 3 diazoles), which are commonly found in biologically active compounds, such as natural products, protein ligands and pharmaceuticals. The structural unit of pyrazole is rarely found in nature but serves as an important core structure of many pharmaceuticals with wide range of biological activities such as cholesterol lowering,²⁸ anti-inflammatory,²⁹ anticancer,³⁰ antidepressant, and antipsychotic agents.³¹ As a result, there is a continuing interest in the development of versatile methods to access highly substituted pyrazoles. Here we report, (i) the synthesis of pyrazolyl ligand (*mdpa*) and its $\text{Cu}(\text{I})$ complex, (ii) the use of the new $\text{Cu}(\text{I})$ -complex to selective preparation of Cu_2S NCs, and (iii) the as-synthesized Cu_2S particles were used as catalyst in photo degradation of Congo red (CR).

2. Experimental details

2.1 Chemicals

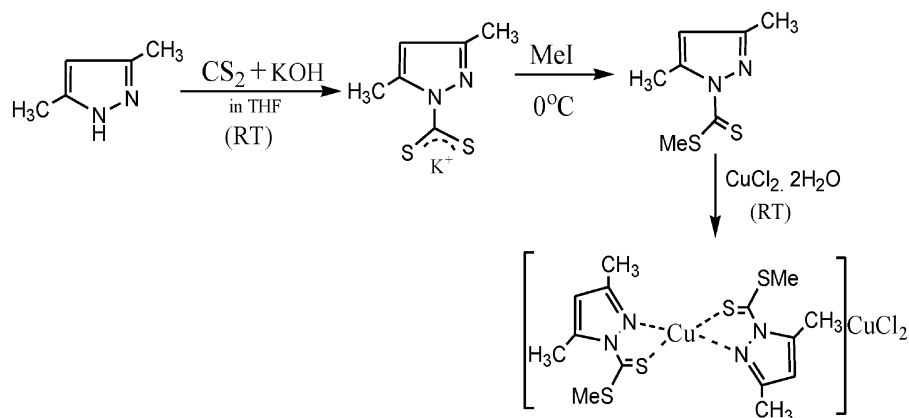
Copper chloride, carbon disulfide (Merck), methyl iodide (Spectrochem), ethylene diamine (Himedia), and ethylene glycol (Himedia), were all analytical grade and used without further purification. Ethanol (Changshu Yangyuan Chemical, China) was dried and distilled before use.

2.2 Synthesis of methyl ester of 3,5-dimethyl pyrazole-1-carbodithioic acid (*mdpa*) and $[\text{Cu}(\text{mdpa})_2][\text{CuCl}_2]$

Carbon disulfide (0.99 g, 13 mmol) was added in a small portion to a mixture of 3,5-dimethylpyrazole (0.97 g, 10.0 mmol) in tetrahydrofuran (15 mL) and finely powdered KOH (0.58 g, 10.3 mmol) at room temperature with constant stirring. The solution turned yellow to orange, and a heavy mass of 3,5-dimethyl pyrazole-1-carbodithioic acid (*dpc*) separated out, which was immediately filtered and thoroughly washed with diethyl ether and dried *in vacuo* over P_4O_{10} . 3.18 g (15 mmol) of properly dried *dpc* was dissolved in 50 mL of distilled water in a 250 mL round bottom flask and placed in an ice bath (0 °C). Methyl iodide (1 mmol, 2.12 g) was slowly added and dropwise for a period of 30 minutes to an aqueous solution (50 mL) of *dpc* (3.18 g, 15 mmol) with constant stirring. The stirring was continued for an additional 1 h, and a yellow colour compound of methyl ester of 3,5-dimethyl pyrazole-1-carbodithioic acid (*mdpa*) separated out, filtered off, washed with water and dried over silica gel. Yield: 82%. M.P. (decomposed): 30 °C. Anal. calc. for $\text{C}_7\text{H}_{10}\text{N}_2\text{S}_2$: C, 45.13; H, 5.41; N, 15.04; S, 34.42. Observed: C, 45.01; H, 5.72; N, 15.48; S, 33.88. IR (cm^{-1}): 3398–3476, $\nu(\text{O-H})$; 980, $\nu(\text{C=S})$; 1575, $\nu(\text{C=N})$; 1490, $\nu(\text{C-N})$.

$\text{CuCl}_2 \cdot 2\text{H}_2\text{O}$ (10 mmol, 1.70 g) dissolved in 20 mL of ethanol was added dropwise to an ethanolic solution of *mdpa* (10 mmol, 1.86 g) dissolved in 20 mL ethanol with constant stirring. Stirring was continued for another half an hour, and a deep blue colour compound separated out. The precipitate formed was filtered, washed with excess ethanol and dried in an oven at 90 °C.

Yield: 80%, mass spectrum *m/z* value: 435.10 (molecular ion peak). Anal. calc. for $\text{C}_{14}\text{H}_{20}\text{C}_{12}\text{N}_4\text{S}_4\text{Cu}_2$: C, 29.47; H, 3.53; N, 9.82; S, 22.48%. Observed: C, 29.46; H, 3.05; N, 9.70; S, 22.78%.



Scheme 1 Synthesis of the ligand and the SP.

The chemical reaction for the preparation of the precursor is detailed in Scheme 1.

2.3 Preparation of copper sulfide nanoparticles using $[\text{Cu}(\text{mdpa})_2][\text{CuCl}_2]$

In a solvothermal synthesis, 0.285 g (0.5 mmol) of the as-prepared precursor, $[\text{Cu}(\text{mdpa})_2][\text{CuCl}_2]$, was taken with 15 mL of solvent in a 50 mL two-necked round bottom flask equipped with a condenser and thermocouple adaptor. The flask was degassed at room temperature for 5 minutes and then filled with inert nitrogen gas. The resulting solution was then gradually heated to 150 °C, and reaction temperature was maintained for 30 minutes. The same set of experiments was also performed at 180 °C for 1 h. The black precipitate formed was collected through centrifugation and was washed for 4–5 times with ethanol. Dry powder copper sulfide NCs were collected by evaporating ethanol at 100 °C for 1 h in an oven.

2.4 Characterization

The single-crystal X-ray diffraction was carried out on a Bruker SMART APEX II X-ray diffractometer equipped with graphite-monochromated Mo-K α radiation ($\lambda = 0.71073 \text{ \AA}$) and 16 CCD area detector. The intensity data were collected in the π and ω scan mode, operating at 50 kV, 30 mA at 296 K.³² The data reduction was performed using the SAINT and SADABS programs.³³ All calculations in the structural solution and refinement were performed using the Bruker SHELXTL program.³⁴ The structure was solved by the heavy atom method and refined by full-matrix least-squares methods. All the non-hydrogen atoms were refined anisotropically; the hydrogen atoms were geometrically positioned and fixed with isotropic thermal parameters. The final electron density maps showed no significant difference. Mass spectra of both ligand and metal complex were obtained using a Waters HRMS XEVO-G2QTOF#YCA351. The elemental analysis (C, H, N, and S) of the complex was performed using a FISON EA-1108 CHN analyzer. The IR spectra (4000–500 cm^{-1}) were recorded on a Perkin Elmer Spectrum Two FT-IR Spectrophotometer with sample prepared as KBr pellets. TG analysis was carried out on a TGA NETZSCH TG 209 F1 instrument at a heating rate of

10 °C min^{-1} under nitrogen. UV-Visible absorption spectra of the samples were recorded on a Perkin Elmer Lambda 35 spectrophotometer in the wavelength range region 200–800 nm at room temperature. Powder X-ray diffraction (XRD) of NCs was recorded using a Seifert XDAL 3000 diffractometer using graphite-monochromated Cu-K α radiation ($\lambda = 1.5418 \text{ \AA}$) with a scan rate 5° min^{-1} over a range of $5^\circ < 2\theta < 80^\circ$ with steps of 0.02° and scintillation detector is operating at 40 kV and 40 mA. TEM and HRTEM of copper sulfide NPs were characterized using a FEI Tecnai G2 T-20S at an accelerating voltage 200 kV. The TEM samples were prepared by placing a drop of a dilute ethanol dispersion of NCs on the surface of a 200-mesh carbon-coated copper grid. The SEM and FESEM images of NCs were acquired with a Gemini Zeiss Supra 40VP (Carl Zeiss Micro imaging GmbH, Berlin, Germany) field emission scanning electron microscope (FESEM) with a 20 kV accelerating voltage. Energy dispersive X-ray (EDX) analysis of the sample was carried out on an Oxford instrument INCA attached to the SEM in the scanning range of 20 keV. Photocatalytic activity of Cu_2S was studied with a 50 mL of $0.5 \times 10^{-3} \text{ M}$ aqueous solution of CR in a 100 mL beaker using visible light source. Further, a 250 W indoor fluorescent lamp was used as light source. To test the photocatalytic degradation of CR, a solution of known CR concentration and Cu_2S NCs photocatalyst was allowed to achieve adsorption equilibrium for 120 min in the dark. Then the solution was exposed to visible light irradiation under magnetic stirring. At 15 min intervals, 3.5 mL of suspension was sampled and centrifuged to remove the photocatalyst powders. The concentration of the dye after photocatalyst degradation was determined with a UV-Vis spectrophotometer.

3. Result and discussions

3.1 Synthesis and characterization of SP with X-ray crystallographic study

The selective synthesis of Cu_2S morphology could be possible with an internally active Cu(I)-precursor in single-source solvothermal route. In search of a new Cu(I) SP, the N-heterocycle-based ligands like pyrazole, imidazole, pyrimidine *etc.* are chosen because of

their special ability to stabilize the lower oxidation states of metal due to their π -acidity.³⁵ Pyrazoles can be used as ligand or as precursors of pyrazole-based ligands and are accessible by well-established synthetic methods.³⁵ These methods are quite general, and this allows the preparation of pyrazoles with a variety of substitution patterns and with different functionalities as substituents of the pyrazole ring. Pyrazole, having two equivalent N-atoms with localized lone pair (σ -donor) on an in-plane orbital and vacant low-lying antibonding π^* orbitals (perpendicular to the molecular plane), shows versatile bonding capabilities with metal ions, and there has been a growing interest in new synthetic methods for the preparation of pyrazole-derived ligands and their metal complexes. A pyrazole-based dithiocarbazate is used to develop a new internally functionalized single-source precursor for copper sulfide nanocrystals. The ligand mdpa and the copper complex were isolated from ethanol in very good yields. It is interesting to note that the solid-state isolation of the Cu(I) complex is possible, starting with a Cu(II) salt *i.e.*, cupric chloride. The sulfur-containing pyrazolyl ligand mdpa reduces Cu(II) to Cu(I) at the same time stabilizes lower oxidation state of copper in the reaction condition.³⁶ The compounds are microcrystalline, stable in air and soluble in some organic solvents.

Fig. 1 shows the FTIR spectra of the free ligand and the copper complex. In order to confirm the mode of bonding of the ligand, the FTIR spectra of the free ligand and the copper complex were studied and assigned based on careful comparison of metal complexes with that of the free ligand. The peaks in the spectrum of the complex are less in number and quite sharp than that of ligand spectrum clearly proving the strong bonding of the ligand(s) with metal. A very broad band typical of water in the 3476–3398 cm^{-1} region is a proof of the hygroscopic nature of the ligand. The ligand shows the bands assigned to $\nu(\text{C}=\text{N})$ and $\nu(\text{C}-\text{N})$ at 1586 cm^{-1} and 1324 cm^{-1} , respectively. An increase in $\nu(\text{C}-\text{N})$ in the free ligand spectrum by *ca.* $\Delta\nu = 7 \text{ cm}^{-1}$ upon complex formation [$\nu(\text{C}-\text{N}) = 1331 \text{ cm}^{-1}$ in complex], as well as an increase ($\Delta\nu = 55 \text{ cm}^{-1}$) in $\nu(\text{C}=\text{N})$ indicate a coordination through tertiary pyrazole ring nitrogen atom. The coordination of the thione sulfur atom to the metal

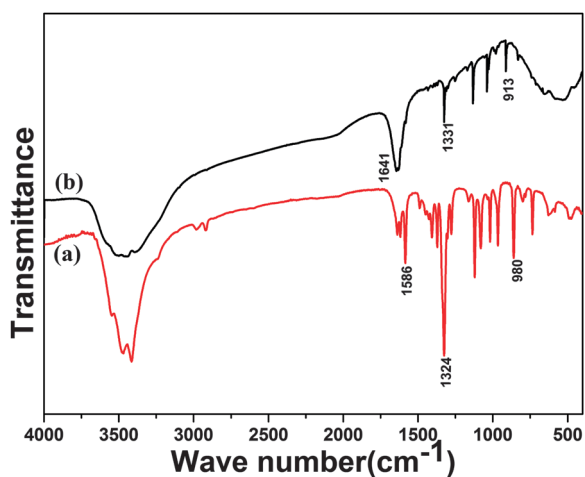


Fig. 1 FTIR spectra of ligand (a) and SP (b).

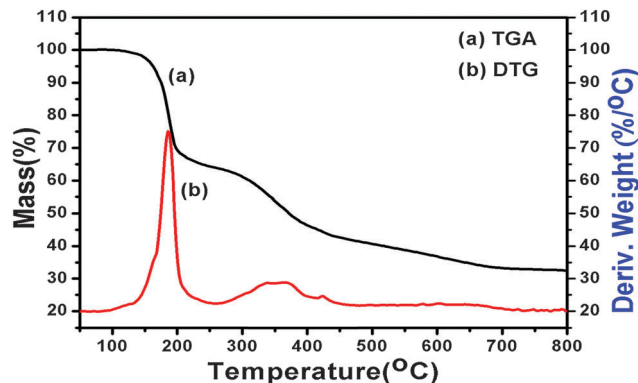


Fig. 2 TGA (a) and derivative of TGA (b) curves for SP.

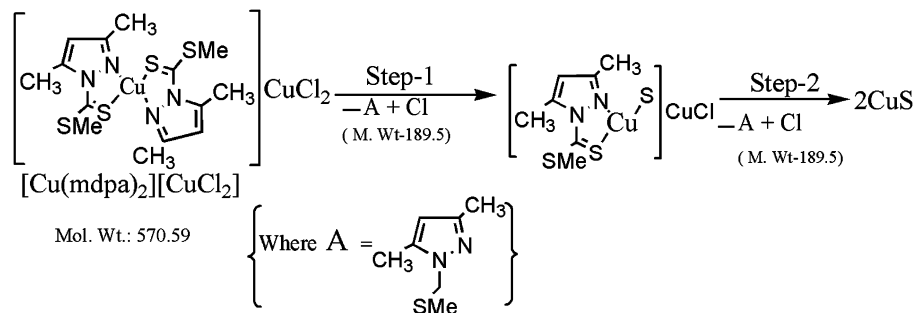
centre is indicated by a decrease of the $\nu(\text{C}=\text{S})$ band from 980 cm^{-1} (in free ligand) to 913 cm^{-1} in its complex form.

TG analysis of the complex was conducted to study the thermal behavior and suitability for the preparation of CuS NCs. The decomposition of the complex started near 100 °C as shown in Fig. 2. The complex undergoes significant weight loss of 33% (*ca.* 33.21%) in the first stage between temperatures 100 °C to 200 °C due to the loss of fragment A along with one Cl. The same loss of units (A) and Cl is repeated over a temperature range from 200 °C to 700 °C in the second stage of decomposition, giving a residue, which is close to the value calculated for the mass percentage of bulk CuS (33.38%). The decomposition steps are shown in Scheme 2.

The molecular structure of SP, $[\text{Cu}(\text{mdpa})_2][\text{CuCl}_2]$, has been established by X-ray crystallography. The ORTEP diagram with the atom numbering scheme is shown in Fig. 3. The crystallographic and experimental data for SP are given in Table 1, and the selected bond lengths and angles are given Table 2. The coordination geometry around the Cu-atom is tetrahedral with an N_2S_2 chromophore with the participation of two ligand moieties. Cu(I) is coordinated by the ternary N-atom and thione sulfur of each ligand and CuCl_2 unit is present outside the coordination sphere to satisfy the residual charge. In the complex, the chelate bite angle of $\text{N}(2)-\text{Cu}(1)-\text{S}(1)$ and $\text{N}(12)-\text{Cu}(1)-\text{S}(11)$ are $84.52(7)^\circ$ and $84.39(7)^\circ$, respectively. These angles are much smaller than the ideal tetrahedral angle (109.28°) as well as the other two tetrahedral angles $\text{N}(2)-\text{Cu}(1)-\text{N}(12)$ [$108.3(10)^\circ$] and $\text{S}(1)-\text{Cu}(1)-\text{S}(11)$ [$121.61(3)^\circ$]. The lowering of the biting angles is due to the closeness of the coordinating N and S atoms in the ligand with a view to facilitate the formation of 5-membered chelate rings. The biting angle $\text{N}(2)-\text{Cu}(1)-\text{N}(12)$ [$108.3(10)^\circ$] reveals that the out-of-plane position of the two adjacent pyrazole rings leads to less steric crowding among methyl groups at the 3(5) position. Thus, the distorted tetrahedral complex becomes vulnerable to ligand substitution prior to formation of the nanoparticle.

3.2 Formation and characterization of Cu_2S NCs

Reaction below the decomposition temperature of the SP (*ca.* 100 °C) leads to an incomplete dissociation of the intermediate species and rendered quite aggregated product. Thus, a higher reaction temperature than the decomposition temperature of SP was considered



Scheme 2 Decomposition steps of the SP in the TG analysis.

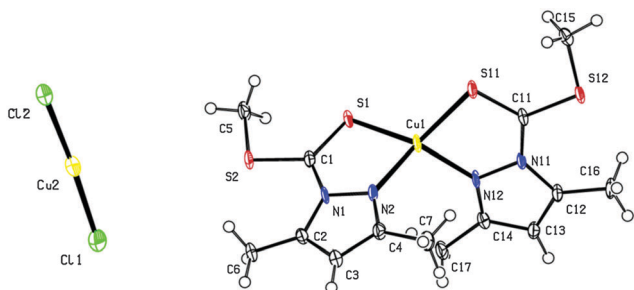


Fig. 3 Coordination environment of the copper atom in the structure of SP.

Table 1 Crystallographic and experimental data for the SP

Empirical formula	C ₁₄ H ₂₀ C ₁₂ Cu ₂ N ₄ S ₄
Formula weight	570.56
Crystal system	Triclinic
Space group	P $\bar{1}$
<i>a</i> /Å	10.5271(9)
<i>b</i> /Å	10.7784(9)
<i>c</i> /Å	10.9396(9)
α /°	68.855(4)
β /°	65.795(4)
γ /°	78.787(5)
<i>V</i> /Å ³	1054.33(15)
<i>Z</i>	2
<i>D</i> _{calc.} /mg m ⁻³	1.797
Absorption coefficient/mm ⁻¹	2.674
<i>F</i> (000)	576
Reflections collected	17 096
Independent reflections	5169
<i>R</i> (int)	0.0613
Theta(deg)	28.30° (98.6%)
<i>R</i> ₁ , <i>wR</i> ₂ [<i>I</i> > 2σ(<i>I</i>)]	0.0526, 0.1342
<i>R</i> ₁ , <i>wR</i> ₂ (all data)	0.0599, 0.1420
Largest diff. peak and hole/e Å ⁻³	1.490, -2.156

with heating durations of 30 minutes or 1 h. The particles obtained in a certain reaction temperature with 30 minutes heating duration were microcrystalline in nature, and the crystallinity improved with increasing the reaction time up to 1 h. It was found that only high chalcocite (Cu₂S) is the product at any reaction temperature irrespective the solvent used in the experiment. The solventless synthesis *i.e.*, heating of SP in a closed quartz furnace in a N₂ atmosphere also gave Cu₂S NCs. Therefore, SP with Cu(I) in its coordination sphere had total control on the product stoichiometry of the copper sulfide NCs, and a further use of any reducing agent/solvent to synthesize Cu₂S from Cu(II) salts or its complexes was not essential.

Table 2 Selected bond length (Å) and bond angles (°) for the SP

Bonds	Values (Å)	Bonds	Values (Å)	Bonds	Values (Å)
C(5)–H(5A)	0.9800	C(5)–H(5B)	0.9800	C(5)–H(5C)	0.9800
C(6)–H(6A)	0.9800	C(6)–H(6B)	0.9800	C(6)–H(6C)	0.9800
S(11)–C(11)	1.666(3)	S(12)–C(11)	1.719(3)	S(12)–C(15)	1.801(3)
N(11)–C(11)	1.390(4)	N(11)–N(12)	1.396(3)	N(11)–C(12)	1.398(3)
N(12)–C(14)	1.308(4)	C(12)–C(13)	1.364(4)	C(12)–C(16)	1.489(4)
Angles	Values (°)	Angles	Values (°)		
N(12)–Cu(1)–N(2)	108.30(10)	N(12)–Cu(1)–S(1)	130.53(7)		
N(2)–Cu(1)–S(1)	84.52(7)	N(12)–Cu(1)–S(11)	84.39(7)		
N(2)–Cu(1)–S(11)	133.25(7)	S(1)–Cu(1)–S(11)	121.61(3)		
Cl(1)–Cu(2)–Cl(2)	175.70(4)	C(1)–S(1)–Cu(1)	99.51(10)		
C(1)–S(2)–C(5)	102.46(14)	C(1)–N(1)–N(2)	117.2(2)		
C(1)–N(1)–C(2)	132.8(2)	N(2)–N(1)–C(2)	109.9(2)		
C(4)–N(2)–N(1)	106.2(2)	C(4)–N(2)–Cu(1)	135.6(2)		
N(1)–N(2)–Cu(1)	116.89(19)	N(1)–C(1)–S(1)	121.2(2)		
N(1)–C(1)–S(2)	115.9(2)	S(1)–C(1)–S(2)	122.89(18)		

The XRD patterns of the samples prepared in EN and EG at 180 °C are shown in the Fig. 4(a) and (b), respectively. All these patterns show four broad peaks at 37.7°, 46.5°, 48.6°, 54.4° and 55.2°, originating from the (102), (110), (103), (112) and (201) lattice plane, which are very close to those reported for chalcocite Cu₂S (JCPDS card 26-1116), with the *p*6₃ space group and a primitive unit cell with *a* = 3.961 Å and *c* = 6.722 Å.

The morphologies of the as-prepared samples were investigated by scanning and transmission electron microscopy. The morphology of the Cu₂S NCs prepared at different temperatures using different solvents was characterized by SEM and FE-SEM and presented in the Fig. 5. Fig. 5(A) and (B) show the SEM and FE-SEM images of the products obtained in EN at 150 °C, respectively. The morphology of Cu₂S product is found to be a cluster of nanocrystals [Fig. 5(A)]. The FE-SEM image shows clusters comprised of nanoplates with hexagonal morphology. The energy dispersive X-ray (EDX) spectrum of this sample shows a 2 : 1 Cu : S atomic ratio, indicating a high chalcocite phase, as shown in Fig. 6. Further increasing the synthesis temperature to 180 °C in the same solvent (EN), achieved a similar Cu₂S cluster, with a diameter range of 0.1–0.2 μm, and these are found to be less compact and the formation of uniform nanoplates is prominent in the SEM [Fig. 5(C)] and FE-SEM [Fig. 5(D)] images. SEM and FE-SEM images of the Cu₂S NCs synthesized from SP in EG at 150 °C clearly shows the agglomerated cluster of both sphere-like nanoparticles and nanoplates with a high degree of

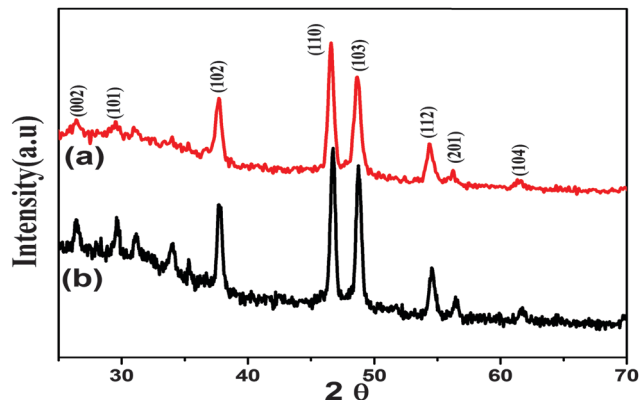


Fig. 4 X-ray diffraction patterns of Cu_2S NCs prepared from SP in EN (a) and in EG (b).

porosity. The degree of porosity and crystallinity increased when the reaction temperature was increased to 180°C as shown in the Fig. 5(G) and (H), and the nanoplates morphologies was prominent over the nanoparticles. Therefore, the use of SP in the solvothermal synthesis of Cu_2S furnishes porous clusters consisting of hexagonal nanoplatelets irrespective of the solvent used in the reaction. It is to be noted that the crystallinity and porosity increased with increasing the reaction temperature. As a result, remarkable photocatalytic activity was shown by the synthesized Cu_2S NCs. For which, the experimental details are discussed later.

Fig. 7 shows the TEM and HRTEM images of the samples prepared at different reaction conditions. When EN is employed as solvent at 150°C for 1 h, the obtained copper sulfide NCs looked spherical with size of 5–7 nm [Fig. 7(A)]. Fig. 7(B) shows a high magnification TEM image of NCs obtained at 180°C . Hexagonal nanoplates are found along with the elongated NCs, and the size of these elongated NCs and hexagonal plates were measured to be in the range of 60–100 nm. The measured lattice spacing of 1.98 Å is well matched to the spacing between the (110) planes of chalcocite Cu_2S [Fig. 7(C)]. Further hydrothermal synthesis of Cu_2S NCs in EG,

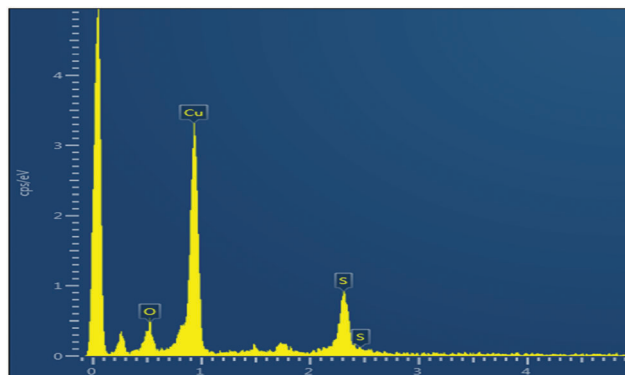


Fig. 6 EDX spectrum of sample prepared in EN at 150°C .

the product morphology is found to be nearly same as that obtained in EN. Nearly spherical particles are found in the product obtained at 150°C in EG [Fig. 7(D)]. However, the low magnified TEM image [Fig. 7(E)] clearly shows primarily hexagonal nanoplates in the size range 40–60 nm along with a few elongated particles. The measured lattice spacing between the (110) planes of Cu_2S is 1.98 Å [Fig. 7(F)].

The optical properties were measured using UV-Vis spectrophotometry. Fig. 8 shows the plot of absorbance vs. wavelength for the Cu_2S NCs prepared in EN and EG at 180°C . A broad peak is observed in the visible region with long trail. The band gap plots of $(\alpha h\nu)^2$ vs. $E(=h\nu)$ as per Tauc's equation [$k(h\nu - E_g)^{1/2}$] for the direct band gap are given in the inset of Fig. 8. The measure band gap is 1.8 eV for Cu_2S prepared in EN, whereas it is 2.4 eV for Cu_2S prepared in EG. This result indicates that the Cu_2S NCs have a suitable band gap for photocatalytic decomposition of organic contaminants under visible light irradiation.

3.3 Photocatalytic activity study of Cu_2S NCs

It is of great importance to investigate the adsorption process of organic pollutants on the catalyst surface to clarify the

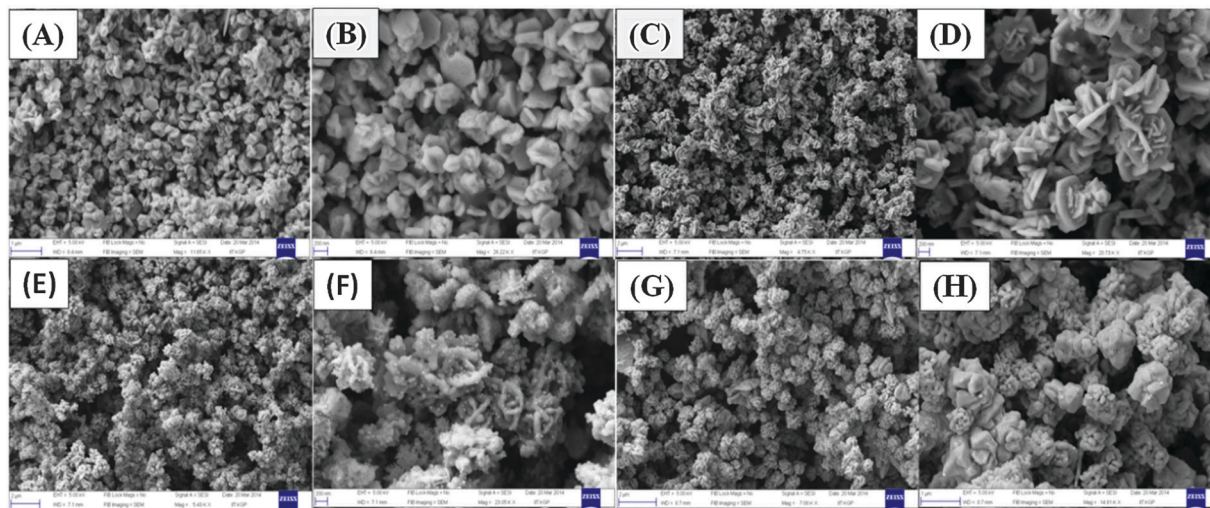


Fig. 5 SEM (A) and FE-SEM (B) of Cu_2S NCs prepared at 150°C in EN; SEM (C) and FE-SEM (D) of Cu_2S NCs prepared at 180°C in EN; SEM (E) and FE-SEM (F) of Cu_2S NCs prepared at 150°C in EG; SEM (G) and FE-SEM (H) of Cu_2S NCs prepared at 180°C in EG.

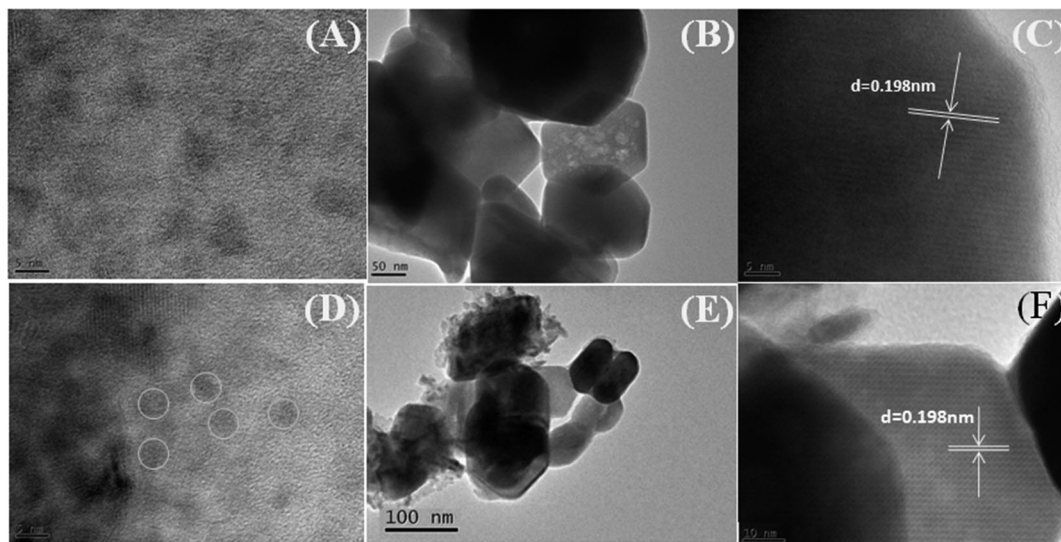


Fig. 7 TEM (A) of Cu_2S NCs prepared at 150 °C in EN; TEM (B) and HRTEM (C) of Cu_2S NCs prepared at 180 °C in EN. HRTEM (D) of Cu_2S NCs prepared at 150 °C in EG; TEM (E) and HRTEM (F) of Cu_2S NCs prepared at 180 °C in EG.

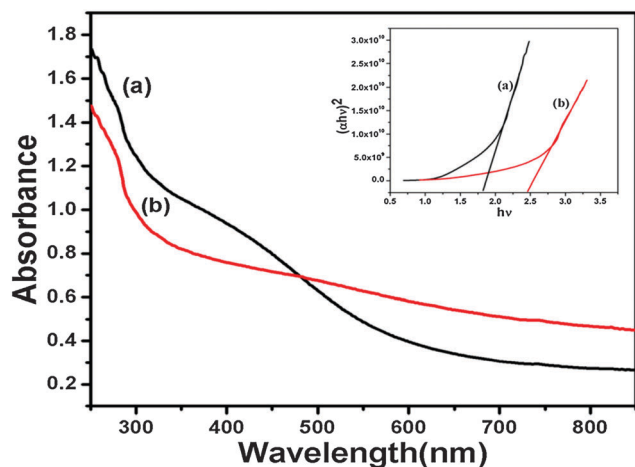


Fig. 8 UV-Vis absorption spectra of samples prepared from EN (a) and EG (b).

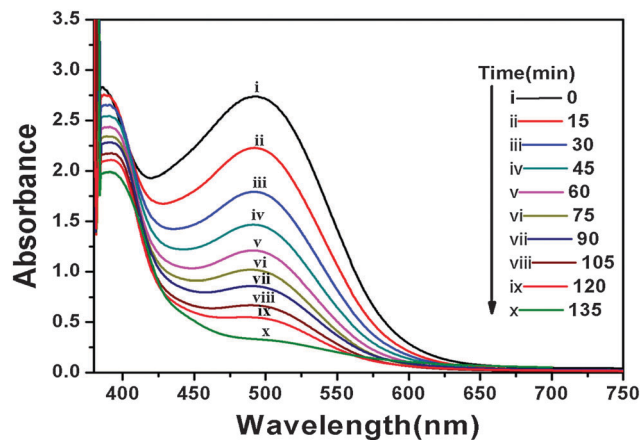


Fig. 9 Time-dependent spectral changes of CR aqueous solution by Cu_2S NCs.

mechanism of photocatalytic reactions, which can facilitate their applications in contaminant destruction. To check the potential of the as-prepared Cu_2S NCs as a photocatalyst, the catalytic performance of Cu_2S NPs were examined by the photodegradation of CR fluorescence dye under the illumination of light followed by spectrophotometric monitoring. The intensity of characteristic absorption peak of CR at 495 nm is remarkably reduced in the presence of Cu_2S NCs upon visible light irradiation with time as shown in Fig. 9. Fig. 10 displays the photodegradation of CR over Cu_2S NCs as a function of $\ln(C_t/C_0)$ vs. irradiation time (min) under visible light illumination. For CR concentration of 0.36 mg L^{-1} , the degradation was almost completed after illumination for 135 minutes. It seemed that the Cu_2S nanoclusters act as good catalyst in the UV-photocatalytic degradation of aqueous solution of CR. The linear relationship between $\ln C_0/C_t$ and time demonstrated that the photocatalytic degradation of CR followed a first-order kinetics: $\ln C_0/C_t = kt$, where k value was calculated as

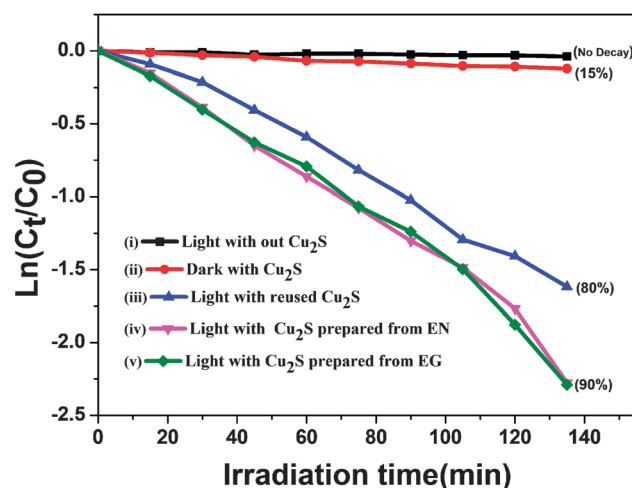


Fig. 10 Logarithmic change in concentration of CR as a function of irradiation time.

$14.05 \times 10^{-3} \text{ min}^{-1}$. To our knowledge, the degradation of CR using Cu_2S NCs was not checked earlier.

Interestingly, the reusability study of the Cu_2S nanocluster catalyst shows 80% degradation of CR as shown in Fig. 10. This proves that the presence of complex internal cavities in the flower like cluster of NCs, which restricts the easy removal of absorbed impurities on the catalytic surface.

Conclusion

A new single source precursor derived from pyrazolyl dithiocarbamate ligand has been used to selectively synthesize hexagonal Cu_2S nanoparticles. The presence of the +1 oxidation state of copper is helpful for the selective synthesis of Cu_2S . The structure of the $\text{Cu}(\text{I})$ complex precursor was solved by single-crystal X-ray crystallography and TG analysis of the precursor was performed to check the suitability of the compound for the synthesis of copper sulfide nanoparticles. The distorted shape, the tetrahedral complex of $\text{Cu}(\text{I})$ and the low decomposition temperature (100°C) facilitate the formation of flower-like hexagonal chalcocite (Cu_2S) nanostructures with sufficient porosity and crystallinity in solvothermal process. Furthermore, the Cu_2S nanoparticles have also been used as catalyst for the photodegradation of aqueous solutions of Congo red (CR) with an efficiency of 90% as well as the reusable catalytic efficiency of Cu_2S is found to be 80%. Further studies on heterocyclic-based precursor will explore the structure and activity relationship for the rational synthesis of other Cu^{I} chalcogenide/chalcogenolate nanoparticles/thin films and their photocatalytic activities.

Acknowledgements

We gratefully acknowledge the research grant from CSIR, Government of India [grant no. 1(2534)/11/EMR-II], and UGC, Government of India [F 42-280/2013(SR)]. We are thankful to Professor Dipankar Chattopadhyay, Department of Polymer Science & Technology, Calcutta University and the people of CRNN, Calcutta University for TEM and SEM picture. Sang Il Seok thanks the Global Research Laboratory (GRL) Program and the Global Frontier R&D Program on Center for Multiscale Energy System funded by the National Research Foundation under the Ministry of Education, Science and Technology of Korea, and by a grant from the KRICT 2020 Program for Future Technology of the Korea Research Institute of Chemical Technology (KRICT), Republic of Korea.

References

- D. Fan, M. Afzaal, M. A. Mallik, C. Q. Nguyen, P. O'Brien and P. J. Thomas, *Coord. Chem. Rev.*, 2007, **251**, 1878–1888.
- B. I. Kharisov, O. V. Kharissova and U. O. Mendez, *J. Coord. Chem.*, 2013, **66**, 3791–3828.
- G. Kedarnath and V. K. Jain, *Coord. Chem. Rev.*, 2013, **257**, 1409–1435.
- J. Kundu and D. Pradhan, *New J. Chem.*, 2013, **37**, 1470–1478.
- Y. Wu, C. Wadia, W. Ma, B. Sadtler and A. P. Alivisatos, *Nano Lett.*, 2008, **8**, 2551–2555.
- C. H. Lai, M. Y. Lu and L. J. Chen, *J. Mater. Chem.*, 2012, **22**, 19–30.
- Y. Xie, L. Carbone, C. Nobile, V. Grillo, S. D'Agostino, F. D. Sala, C. Giannini, D. Altamura, C. Oelsner, C. Kryschi and P. D. Cozzoli, *ACS Nano*, 2013, **7**, 7352–7369.
- L. Reijnen, B. Meester, A. Goossens and J. Schoonman, *Chem. Vap. Deposition*, 2003, **9**, 15–20.
- M. C. Lin and M. W. Lee, *Electrochem. Commun.*, 2011, **13**, 1376–1378.
- L. Chen, Y. D. Xia, X. F. Liang, K. B. Yin, J. Yin, Z. G. Liu and Y. Chen, *Appl. Phys. Lett.*, 2007, **91**, 073511.
- T. Sakamoto, H. Sunamura, H. Kawaura, T. Hasegawa, T. Nakayama and M. Aono, *Appl. Phys. Lett.*, 2003, **82**, 3032.
- L. Zhao, F. Tao, Z. Quan, X. Zhou, Y. Yuan and J. Hu, *Mater. Lett.*, 2012, **68**, 28–31.
- A. A. Sagade, R. Sharma and I. Sulaniya, *J. Appl. Phys.*, 2009, **105**, 043701.
- S. Goel, F. Chen and W. Cai, *Small*, 2014, **10**, 631–645.
- Z. P. Liu, D. Xu, J. B. Liang, J. M. Shen, S. Y. Zhang and T. Y. Qian, *J. Phys. Chem. B*, 2005, **109**, 10699–10704.
- W. Lou, M. Chen, X. Wang and W. Liu, *J. Phys. Chem. C*, 2007, **111**, 9658–9663.
- X. S. Du, Z. Z. Yu, A. Dasari, J. Ma, Y. Z. Meng and Y. W. Mai, *Chem. Mater.*, 2006, **18**, 5156–5158.
- M. B. Sigman, A. Ghezelbash, T. Hanrath, A. E. Saunders, F. Lee and B. A. Korgel, *J. Am. Chem. Soc.*, 2003, **125**, 16050–16057.
- X. H. Li, J. X. Li, G. D. Li, D. P. Liu and J. S. Chen, *Chem. – Eur. J.*, 2007, **13**, 8754–8761.
- P. Roy and S. K. Srivastava, *Cryst. Growth Des.*, 2006, **6**, 1921–1926.
- T. Mandal, G. Piburn, V. Stavila, I. Rusakova, T. O. Ely, A. C. Colson and K. H. Whitmire, *Chem. Mater.*, 2011, **23**, 4158–4169.
- Y. Lou, A. C. S. Samia, J. Cowen, K. Banger, X. Chen, H. Lee and C. Burda, *Phys. Chem. Chem. Phys.*, 2003, **5**, 1091–1095.
- S. Gorai, D. Ganguli and S. Chaudhuri, *Cryst. Growth Des.*, 2005, **5**, 875–877.
- P. Bera and S. I. Seok, *Solid State Sci.*, 2012, **14**, 1126–1132.
- Y. Xie, A. Riedinger, M. Prato, A. Casu, A. Genovese, P. Guardia, S. Sottini, C. Sangregorio, K. Miszta, S. Ghosh, T. Pellegrino and L. Manna, *J. Am. Chem. Soc.*, 2013, **135**, 17630–17637.
- D. Dorfs, T. Hartling, K. Miszta, N. C. Bigall, M. R. Kim, A. Genovese, A. Falqui, M. Povia and L. Manna, *J. Am. Chem. Soc.*, 2011, **133**, 11175–11180.
- P. S. Nair and G. D. Scholes, *J. Mater. Chem.*, 2006, **16**, 467–473.
- D. R. Sliskovic, B. D. Roth, M. W. Wilson, M. L. Hoefle and R. S. Newton, *J. Med. Chem.*, 1990, **33**, 31–38.
- T. D. Penning, J. J. Talley, S. R. Bertenshaw, J. S. Carter, P. W. Collins, S. Docter, M. J. Graneto, L. F. Lee,

- J. W. Malecha, J. M. Miyashiro, R. S. Rogers, D. J. Rogier, S. S. Yu, G. D. Anderson, E. G. Burton, J. N. Cogburn, S. A. Gregory, C. M. Koboldt, W. E. Perkins, K. Seibert, A. W. Veenhuizen, Y. Y. Zhang and P. C. Isakson, *J. Med. Chem.*, 1997, **40**, 1347–1365.
- 30 S. R. Stauffer and J. A. Katzenellenbogen, *J. Comb. Chem.*, 2000, **2**, 318–329.
- 31 K. W. Moore, K. Bonner, E. A. Jones, F. Emms, P. D. Leeson, R. Marwood, S. Patel, S. Patel, M. Rowley, S. Thomas and R. W. Carling, *Bioorg. Med. Chem. Lett.*, 1999, **9**, 1285–1290.
- 32 Bruker, *SMART (Version 5.625) Data Collection Program*, Bruker AXS Inc., Madison, Wisconsin, USA, 2001.
- 33 Bruker, *SAINTE (Version 6.28a) and SADABS (Version 2.03) Data Reduction and Absorption Correction Program*, Bruker AXS Inc., Madison, Wisconsin, USA, 2001.
- 34 G. M. Sheldrick, *SHELXTL (Version 6.12) Structure Analysis Program*, Bruker AXS Inc., Madison, Wisconsin, USA, 2001.
- 35 J. Perez and L. Riera, *Eur. J. Inorg. Chem.*, 2009, 4913–4925.
- 36 T. N. Mandal, S. Roy, A. K. Barik, S. Gupta, R. J. Butcher and S. K. Kar, *Inorg. Chim. Acta*, 2009, **362**, 1315–1322.